Check for updates

Small Methods

small methods
www.small-methods.com

RESEARCH ARTICLE OPEN ACCESS

Filtration-Based SERS With In Situ Gold Growth in Bacterial Microenvironment for Rapid Detection of Low-Level Bacteria

Eun-Bi Jang[1,2] | Ji Young Lee[1] | Hoeil Chung[2] | Min-Young Lee[1]

[1]Advanced Bio and Healthcare Materials Research Division, Korea Institute of Materials Science (KIMS), Changwon, Gyeongnam, Republic of Korea | [2]Department of Chemistry and Research Institute for Convergence of Basic Science, Hanyang University, Seoul, Republic of Korea

Correspondence: Ji Young Lee (young7277@kims.re.kr) | Hoeil Chung (hoeil@hanyang.ac.kr) | Min-Young Lee (myay0615@kims.re.kr)

Received: 22 May 2026 | **Revised:** 6 July 2026 | **Accepted:** 7 August 2026

Keywords: bacterial microenvironment | filtration-based detection | in situ gold growth | low-level detection | rapid antimicrobial susceptibility testing | surface-enhanced Raman scattering

ABSTRACT

Rapid bacterial detection and timely antimicrobial susceptibility assessment are essential for effective infection management, yet remain challenging under clinically relevant low-concentration conditions. Here, we present a filtration-based surface-enhanced Raman scattering (SERS) platform based on a microenvironment engineering strategy, in which plasmonic nanostructures are dynamically formed within the bacterial microenvironment. Using a gold nanostructured glass microfiber membrane, the platform enables large-volume sample processing through size-selective bacterial capture, followed by in situ gold growth that generates bacteria-centered plasmonic hotspots directly around bacterial cells. This architecture fundamentally overcomes the intrinsic hotspot–bacteria mismatch in conventional substrate-based SERS systems, enabling highly sensitive and selective detection while effectively suppressing nonspecific interference in complex biological matrices. To further address sampling limitations at low concentrations, a minimal pre-culture strategy was introduced to enhance bacterial surface occupancy, improving the detection limit from 10^3 to 10^1 CFU/mL. In addition, SERS signal intensity directly reflects bacterial viability, allowing rapid differentiation of antimicrobial responses and enabling susceptibility assessment within 2 h. By integrating physical enrichment with microenvironment-driven signal amplification, this platform simultaneously achieves low-level detection and rapid antimicrobial susceptibility testing within a single system. These results highlight its potential as a next-generation integrated diagnostic platform for clinical sample analysis.

1 | Introduction

Bacterial infections remain a major global health challenge, particularly in clinical settings where rapid and reliable diagnosis is essential for effective treatment [1]. Among clinically important pathogens, *Escherichia coli (E. coli)* is a leading cause of urinary tract infections (UTI) and is frequently associated with severe systemic infections such as sepsis [2, 3]. In these conditions, early detection of bacterial presence is critical, especially because bacterial burdens are often very low during the initial stages of infection.

A major limitation of current diagnostic approaches is the difficulty of achieving reliable bacterial detection at low concentrations in complex biological matrices such as blood and urine [4, 5]. In early-stage infections, bacterial loads can be as low as 1–100 CFU/mL, where analytical performance is easily compromised by matrix-derived interference, low signal intensity, and poor

This is an open access article under the terms of the Creative Commons Attribution-NonCommercial-NoDerivs License, which permits use and distribution in any medium, provided the original work is properly cited, the use is non-commercial and no modifications or adaptations are made.
© 2026 The Author(s). *Small* Methods published by Wiley-VCH GmbH

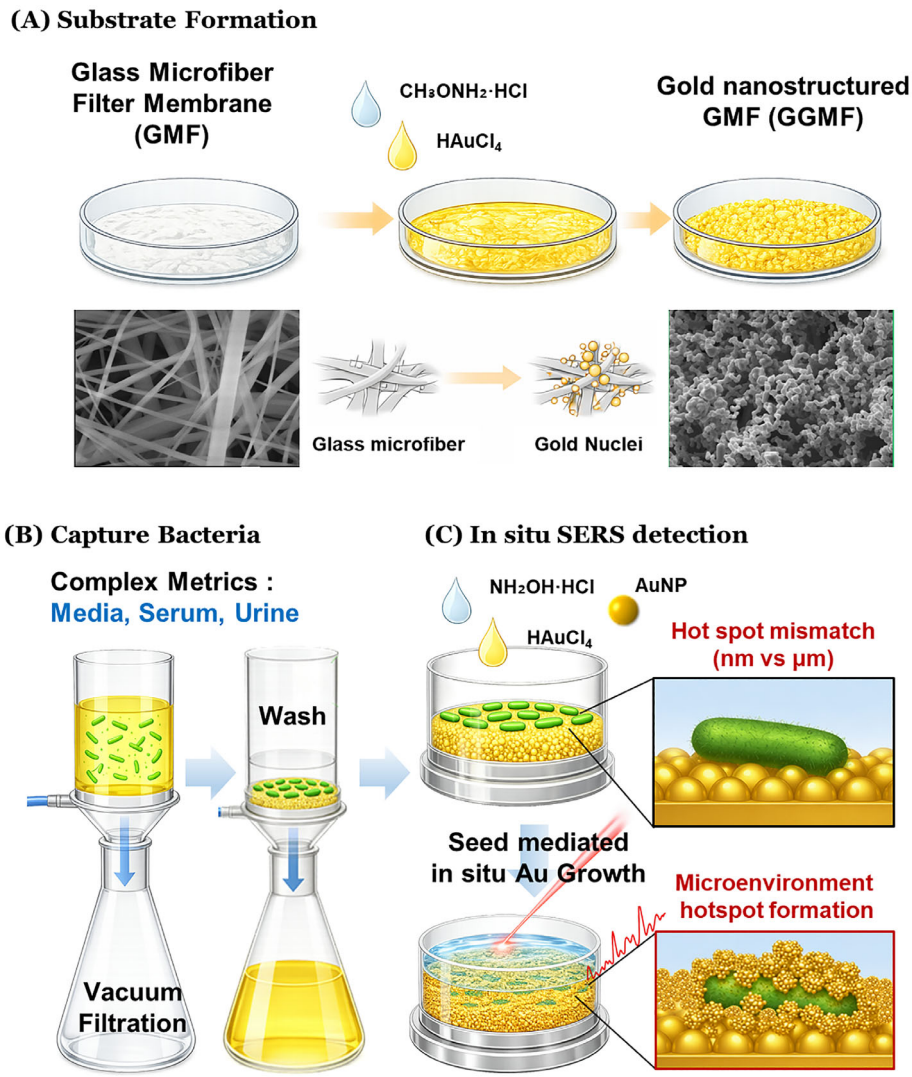

FIGURE 1 | Schematic illustration for the SERS detection of *E. coli* without pre-treatment. (A) Fabrication of the Au nanostructured glass microfiber filter substrate (GGMF). (B) Overall assay workflow of (B) filtration of bacteria on GGMF and (C) in-situ gold growth, and SERS detection.

reproducibility [6, 7]. To address these challenges, conventional methods typically rely on extensive sample preprocessing steps, including centrifugation, filtration, or enrichment, to isolate and concentrate bacterial cells prior to analysis. However, these procedures are time-consuming, require laboratory infrastructure, and are difficult to integrate into automated or point-of-care diagnostic workflows. Molecular and genomic diagnostic approaches have significantly improved the speed of pathogen identification; however, they often rely on the detection of predefined genetic markers and do not necessarily reflect functional antibiotic susceptibility [8–10]. The presence of resistance-associated genes does not always correlate with phenotypic resistance, and emerging or unknown resistance mechanisms may not be captured by targeted assays. Consequently, direct assessment of bacterial behavior under antibiotic exposure remains essential for guiding effective antimicrobial therapy.

Surface-enhanced Raman scattering (SERS) has emerged as a promising analytical technique due to its high sensitivity and ability to provide label-free molecular information [11]. However, its application to the detection of low-abundance bacteria remains challenging, particularly in complex biological fluids such as blood or urine [12]. In such environments, abundant proteins and other interfering components hinder direct detection by inducing nonspecific adsorption and strong background signals. To address this issue, conventional approaches typically employ sample pretreatment steps, such as centrifugation, to isolate and concentrate bacteria, thereby improving detection sensitivity. To reduce these preprocessing steps while maintaining the enrichment effect, filter-based SERS platforms have been reported as a strategy for simultaneous separation and detection [13, 14]. However, despite these efforts, effective signal generation in current SERS-based approaches remains fundamentally constrained. This limitation primarily arises from the inherent mismatch between nanoscale plasmonic hotspots and microscale bacterial structures, which significantly reduces the probability of efficient hotspot–bacteria interactions [15]. As a result, electromagnetic coupling is often inefficient and signal responses become highly variable, particularly under low-concentration conditions. Consequently, even after enrichment or separation, reliable bacterial detection remains difficult in complex biological matrices.

23669608, 2026, 19, Downloaded from https://onlinelibrary.wiley.com/doi/10.1002/smtd.70972 by Hanyang University Library, Wiley Online Library on [27/10/2026]. See the Terms and Conditions (https://onlinelibrary.wiley.com/terms-and-conditions) on Wiley Online Library for rules of use; OA articles are governed by the applicable Creative Commons License

Here, we present a filtration-integrated SERS platform based on a microenvironment-driven plasmonic engineering strategy, enabling dynamic reconstruction of hotspots within the bacterial microenvironment. Following size-selective capture of bacteria using an Au nanostructured glass microfiber filter, in situ gold growth is induced to directly generate plasmonic nanostructures around bacterial cells. Unlike conventional systems that rely on pre-existing substrate hotspots, this approach enables localized hotspot formation at the bacteria–substrate interface, fundamentally resolving the intrinsic hotspot–bacteria mismatch and significantly enhancing electromagnetic coupling and interaction probability (Figure 1). Furthermore, we systematically address a critical yet often overlooked factor in low-level detection: stochastic sampling limitations. Under low bacterial concentrations, detection performance is governed not only by analytical sensitivity but also by the probability of bacterial presence within the laser interrogation area. To overcome this limitation, a minimal pre-culture strategy is introduced to increase bacterial surface occupancy, thereby substantially improving detection reliability without complex sample processing. By integrating physical enrichment, microenvironment-driven hotspot reconstruction, and probabilistic detection control, the proposed platform achieves both high sensitivity and selectivity under clinically relevant conditions. Moreover, as SERS signal intensity directly correlates with bacterial viability, this system enables rapid antimicrobial susceptibility testing (AST), providing functional diagnostic information within a significantly reduced timeframe.

2 | Meterials and Methods

2.1 | Materials

All chemicals were of analytical grade and used without further purification. Gold(III) chloride trihydrate ($HAuCl_4$), hydroxylamine hydrochloride ($HONH_2{\cdot}HCl$), and sodium citrate dihydrate were purchased from Sigma-Aldrich (St. Louis, MO, USA). O-Methylhydroxylamine Hydrochloride (OMH) was obtained from Tokyo Chemical Industry (Tokyo, Japan), Cat. No. M0886. Glass microfiber filter was obtained from WHATMAN (Maidstone, UK), Grade GF/F, 25 mm, Cat. No. 1825-025. The 96-well plate (non-treated, flat bottom) was obtained from SPL Life Sciences Co., LTD (Gyeonggi, South Korea), Cat. No. SPL32096. *Escherichia coli* (KCCM 40271), Staphylococcus aureus and *Klebsiella pneumoniae* (KCCM 40890) were obtained from the Korean Culture Center of Microorganisms (Seoul, South Korea). Tryptic Soy Broth (TSB) was obtained from Difco Laboratories (Detroit, MI, USA), Cat. No. 211825. Fetal Bovine Serum (FBS) was purchased from Welgene (Kyungsan, South Korea), Cat. No. S001-01.

2.2 | Fabrication of Au Nanostructured SERS Filter Membrane

The reaction solution was prepared by mixing a gold precursor ($HAuCl_4$) and a reducing agent (OMH) at a ratio of 1:5, with the $HAuCl_4$ concentration adjusted to 10 mM. The glass microfiber filter (0.7 μm pore size) was immersed in the reaction solution for 16 h at room temperature. Afterward, the filter was washed with deionized (DI) water for 5 min, three times, followed by complete drying at room temperature for 2 h. To quantitatively evaluate the pore size of the GMF and GGMF substrates before and after gold nanostructure formation, SEM images were analyzed using a custom image-processing workflow implemented in Python (OpenCV). Each image was calibrated individually based on its corresponding SEM scale bar to convert pixel dimensions into micrometers. Otsu's thresholding was then applied to automatically segment the microfiber network from the pore regions. The effective pore size was calculated as the equivalent circular diameter of each segmented pore, and more than 50 pores ($n > 50$) were analyzed for each sample condition to determine the average pore size.

2.3 | Synthesis of Colloidal AuNPs (Approximately 50 Nm)

2.3.1 | Synthesis of Au Seeds (~10 nm, ~3×10^{12} NPs/mL)

A 2.2 mM sodium citrate solution (150 mL) was heated to boiling in an Erlenmeyer flask under vigorous stirring for 15 min. Subsequently, 1 mL of $HAuCl_4$ (25 mM) was rapidly injected, inducing a color change from yellow to bluish gray and finally to soft pink within 10 min. The resulting Au seeds were stabilized by citrate ions and remained well-dispersed in water.

2.3.2 | Seeded Growth to ~80 nm AuNPs

The reaction temperature was reduced to 90°C. Sodium citrate (1 mL, 60 mM) and $HAuCl_4$ (1 mL, 25 mM) were then sequentially added within 2 min (Step 1). After 30 min, a 1 mL aliquot was collected for UV–Vis spectroscopy to monitor particle size and concentration. Step 1 was repeated nine times to achieve progressive particle growth up to ~80 nm. The synthesis procedure was adapted from a previously reported method. UV–Vis spectra were recorded after each growth step, and particle size and concentration were determined based on established calibration [16].

2.4 | E. coli Growth and Culture

Frozen stocks of *E. coli* KCCM 40271 were used to inoculate 4 mL of TSB, and the cultures were incubated overnight at 37°C in a rotary thermo-shaker (Gerhardt, Germany) at 150 rpm. The overnight culture was centrifuged at 8000 rpm for 5 min, and the resulting pellet was washed twice and resuspended in sterile deionized water. Cell density was determined by measuring the optical density at 600 nm (OD_{600}) using a UV–Vis spectrophotometer.

2.5 | Filtration of E. coli Using the SERS Filter Membrane

The fabricated SERS membrane was placed on a 25 mm glass-base funnel assembled onto a 250 mL filter flask. The filtration system was connected to a suction pump (Puritech Co., Ltd.,

23669608, 2026, 19, Downloaded from https://onlinelibrary.wiley.com/doi/10.1002/smtd.70972 by Hanyang University Library, Wiley Online Library on [27/10/2026]. See the Terms and Conditions (https://onlinelibrary.wiley.com/terms-and-conditions) on Wiley Online Library for rules of use; OA articles are governed by the applicable Creative Commons License

Gyeonggi, South Korea) using a vacuum filtration holder kit (DWK Life Sciences, NJ, USA). *E. coli* was spiked into FBS, TSB, urine, and deionized (DI) water, and the final volume of each sample was adjusted to 5 mL. For quantitative studies, the concentration of bacteria was varied from 10 CFU/mL to 10^7 CFU/mL. The prepared samples were directly subjected to vacuum filtration. Subsequently, 5 mL of DI water was filtered through the membrane twice to remove residual components.

2.6 | In Situ Gold Growth on the Filtrated SERS Filter Membrane

The filtrated SERS membrane was placed in a plastic well. Subsequently, deionized (DI) water, AuNP solution, hydroxylamine hydrochloride (HH, 500 mM), and $HAuCl_4$ (50 mM) were sequentially added (50 μL each) to induce in situ gold growth on the membrane. The reaction was allowed to proceed at room temperature for 1 h 40 min.

2.7 | SERS Measurement

SERS spectra were acquired from the bacteria-captured SERS membranes during the in situ gold growth process without removing the reaction solution. Measurements were performed using a portable spectrometer (QEPro Raman, Ocean Optics, USA) equipped with a 785 nm laser (40 mW), with an integration time of 60 s. This configuration enabled real-time monitoring during the gold growth process. After the in situ gold growth process (1 h 40 min), SERS spectra were collected in the fingerprint region (400–1800 cm^{-1}) at five randomly selected positions on each sample.

2.8 | Comparison of Vacuum Filtration and Drop-Casting Methods

Vacuum filtration was performed as described in Section 2.5. For the drop-casting method, 20 μL of the bacterial suspension was directly dispensed onto a 6-mm-diameter GGMF membrane and allowed to dry at room temperature (drop-casting without Au growth). For the Au growth group, in situ Au growth was subsequently performed on the drop-casted samples according to the procedure described in Section 2.6 (drop-casting with Au growth). Subsequently, SERS spectra were acquired under identical measurement conditions, and the performance of the vacuum filtration and drop-casting methods was comparatively evaluated.

2.9 | Minimal Culture Test for Detection of Low Concentration

In clinical practice, serum samples are often mixed with culture media for diagnostic testing. To mimic these conditions, FBS and TSB were mixed at a 1:1 volume ratio to a final volume of 5 mL. *E. coli* was spiked into the FBS–TSB mixture at concentrations ranging from 10 to 10^4 CFU/mL and incubated for 0–4 h at 37°C under gentle agitation in 50 mL conical tubes.

2.10 | AST

To evaluate the antibiotic response of *E. coli*, bacteria (1×10^3 CFU/mL) were treated with amikacin and ampicillin (1 mg/mL each) in TSB at 37°C under gentle agitation for designated time points (approximately 30 min to 4 h). Samples were subsequently analyzed by SERS following the previously described protocol.

2.11 | Bacterial Discrimination via Principal Component Analysis (PCA)

Escherichia coli (E. coli), *Staphylococcus aureus (S. aureus)*, and *Klebsiella pneumoniae (Klebsiella spp.)* were prepared at a concentration of 1×10^7 CFU/mL, individually filtered through the GGMF, and subjected to in situ Au growth as described in Sections 2.5 and 2.6. SERS spectra were subsequently acquired under identical measurement conditions. For objective spectral comparison, all spectra were normalized by scaling the maximum peak intensity to one (Max = 1). The normalized spectral datasets were analyzed by principal component analysis (PCA) using the Scikit-learn library in Python. The resulting principal components were visualized as two-dimensional score plots, and 95% confidence ellipses were plotted to evaluate the separation among the bacterial groups.

2.12 | Data Processing and Analysis

SERS spectra were processed using Origin 2022b. For each sample, spectra were collected from five random spots, and the intensity at 730 cm^{-1} was averaged. Reproducibility was assessed by one-way ANOVA ($p < 0.05$). Measurement precision was evaluated using the relative standard deviation (RSD, %).

3 | Result and Discussion

3.1 | Fabrication of the Au Nanostructured SERS Filter Membrane

To enable rapid detection of bacteria in complex biological matrices while minimizing extensive sample pretreatment, we designed a SERS-based strategy that integrates filtration-assisted bacterial capture with in situ growth of gold nanostructures around the bacterial microenvironment. Successful implementation of this approach requires the selection of a filter material that enables efficient bacterial capture while providing a low background signal.

To this end, three commercially available filter materials—polytetrafluoroethylene (PTFE), cellulose acetate (CA), and glass microfiber (GMF)—were evaluated as candidates (Figure S1). Gold nanostructures were formed on each filter via a solution-based reduction process using $HAuCl_4$ and O-methylhydroxylamine hydrochloride (OMH). This method allows facile and uniform formation of gold nanostructures without the need for sophisticated equipment, while enabling precursor infiltration throughout the porous filter network to generate three-dimensional nanostructures [17]. In addition, OMH acts as a mild reducing agent, promoting gradual growth

23669608, 2026, 19, Downloaded from https://onlinelibrary.wiley.com/doi/10.1002/smtd.70972 by Hanyang University Library, Wiley Online Library on [27/10/2026]. See the Terms and Conditions (https://onlinelibrary.wiley.com/terms-and-conditions) on Wiley Online Library for rules of use; OA articles are governed by the applicable Creative Commons License

on pre-existing surfaces rather than rapid nucleation, thereby facilitating the formation of more uniform and reproducible nanostructures. Among the tested materials, PTFE did not support gold nanostructure formation due to its hydrophobic surface (contact angle ~135°), which prevented uniform wetting by the precursor solution and hindered nucleation and growth processes [18]. In contrast, both CA and GMF exhibited hydrophilic surfaces that allowed uniform infiltration of the precursor solution into the filter matrix, enabling gold nanostructure formation along the surface and fibrous network [19, 20].

To evaluate substrate-derived background signals under realistic conditions, SERS spectra were collected after filtration of DI water, followed by an additional gold growth step (Figure S2). This approach reflects the actual filtration environment, where trace residual species and nonspecifically adsorbed components can become concentrated and trapped within the porous filter structure, and subsequently amplified by plasmonic hotspots. As a result, the CA-based SERS filter exhibited relatively strong background signals, whereas the GMF-based SERS filter showed minimal interference. This difference can be attributed to the intrinsic Raman activity of the CA polymer, arising from C = O, C–H, and C–O bonds, whereas the silica-based GMF (Si–O–Si network) exhibits minimal polarizability changes during molecular vibrations and is thus largely Raman-inactive [21–23]. Consequently, GMF minimizes substrate-induced background contributions even in regions not fully covered by gold nanostructures.

Based on these results, GMF was selected as the optimal filter material for SERS-based bacterial detection due to its low background signal and compatibility with gold nanostructure formation. SEM analysis revealed that the fabricated gold nanostructured GMF (GGMF)-based SERS membrane consisted of a three-dimensional network of interconnected spheroidal structural units with an average diameter of 176 ± 26 nm. This morphology provides abundant interparticle junctions and nanoscale gaps, generating strong electromagnetic hotspots. The formation of this structure is attributed to the mild reduction kinetics of OMH. As a relatively slow reducing agent, OMH favors gradual growth on existing nuclei and surfaces rather than rapid, random nucleation. This leads to preferential deposition of gold at energetically favorable sites, particularly around pre-existing nanostructures and bacterial surfaces, resulting in localized accumulation. Such a growth mechanism induces structural evolution resembling interparticle bridging and reorganization, ultimately increasing hotspot density and contributing significantly to SERS signal enhancement.

Quantitative SEM image analysis showed that the average effective pore size decreased from 1.96 to 0.95 μm following in situ Au growth (Figure S3). This result suggests that the Au nanostructures formed conformally along the microfiber surfaces without completely blocking the three-dimensional fibrous network. Capture efficiency analysis using a 5 mL sample demonstrated that the GGMF achieved a bacterial capture efficiency of >99.9% for *E. coli* at initial concentrations of approximately 1.4×10^4 and 1.3×10^6 CFU/mL (Figure S4 and Table S1). These results indicate that the porous structure of the GGMF was well preserved after Au growth while maintaining highly efficient bacterial capture during filtration.

3.2 | In Situ Gold Growth in the Microenvironment Surrounding Bacteria After Filtration for SERS Signal Amplification

Conventional SERS-based bacterial detection suffers from a fundamental limitation arising from the size mismatch between nanoscale plasmonic hotspots and microscale bacterial structures, which restricts efficient interactions at the bacteria–hotspot interface. This structural discrepancy reduces both signal reproducibility and sensitivity due to insufficient hotspot contact with bacterial surfaces.

To address this issue, we propose a strategy that combines filtration-assisted bacterial localization with post-filtration in situ gold nanostructure growth in the microenvironment surrounding the bacteria. Briefly, bacterial suspensions were filtered to capture bacteria onto the GGMF SERS-active membrane, followed by placement of the membrane into a plastic well for subsequent growth. In situ gold growth was then induced by introducing a mixed reaction solution (200 μL) containing AuNPs (~50 nm), $HAuCl_4$, and HH. In this system, AuNPs act as seeds to promote surface-mediated growth, while HH, as a relatively slow reducing agent, preferentially drives growth on pre-existing surfaces rather than homogeneous nucleation, thereby enabling localized nanostructure formation around the bacterial microenvironment [24]. In particular, the presence of AuNP seeds directs the reduction reaction to occur preferentially on the seed surface, allowing effective control over the progression of the reduction process and enhancing localized growth. These conditions are expected to enable stable gold growth while maintaining structural control. In contrast, the use of stronger reducing agents such as sodium borohydride ($NaBH_4$) results in rapid and uncontrolled reduction, leading to excessive homogeneous nucleation and nonspecific particle formation [25]. This, in turn, produces randomly distributed nanostructures and hinders precise hotspot localization. Therefore, HH was selected as the reducing agent to balance growth rate and structural control.

As one of the most common and widely studied bacterial species, *E. coli* was selected as a representative model organism for this study. To investigate the kinetics of in situ gold growth, time-dependent SERS signals were monitored in real time using *E. coli* (1×10^7 CFU/mL, 5 mL) captured on the membrane (Figure 2A). The Raman intensity at 730 cm^{-1} exhibited a gradual increase over time, which is attributed to adenine, a well-known characteristic Raman peak of bacteria [26]. Consistent enhancement of characteristic Raman peaks across the spectrum was also observed (Figure 2B). Quantitative analysis revealed that the 730 cm^{-1} peak reached a maximum intensity at approximately 100 min, followed by a plateau, leading to the selection of 100 min as the optimal reaction time. In addition, comparison with the background signal obtained after DI water filtration followed by in situ growth of Au nanostructures confirmed that the characteristic Raman peaks from *E. coli* were clearly distinguishable from the background (Figure 2C), which is further supported by the summarized spectral features listed in Table 1. To further evaluate

23669608, 2026, 19, Downloaded from https://onlinelibrary.wiley.com/doi/10.1002/smtd.70972 by Hanyang University Library, Wiley Online Library on [27/10/2026]. See the Terms and Conditions (https://onlinelibrary.wiley.com/terms-and-conditions) on Wiley Online Library for rules of use; OA articles are governed by the applicable Creative Commons License

TABLE 1 | *E. coli* Raman peak list with literature-supported assignments.

	Raman shift (cm^{-1})	Proposed assignment	Refs.
1	730	Glycosidic (peptidoglycan, NAG, NAM) and adenine (purine base) ring breathing mode	[36, 38–41]
2	780	DNA/RNA ring breathing (pyrimidine bases) mode, Phosphodiester bands in DNA	[36–39, 42]
3	858	COC stretching of glycosidic linkage, C–C proline stretching, Thymine and tyrosine ring breathing mode	[36–39, 42]
4	890	COC stretching mode (carbohydrates)	[37, 41]
5	959	$\nu(CH_3)$ of proteins (a-helix), (C=C deformation) carotenoid, N–C stretching	[36, 38, 40, 42]
6	1004	Phenylalanine symmetric ring-breathing (aromatic C–C skeletal), carotenoid ν_3 (CH in-plane)	[36, 37, 39, 41–43]
7	1112	DNA, O–P–O DNA backbone	[37, 44]
8	1161	Carotenoid ν_2 (C–C stretching of the polyene chain), C–N and C–C stretching, amide III	[36, 37, 42, 43]
9	1236	$\nu(PO_2^-)$ of Phosphate backbone, minor amide III (C–N stretching and N–H bending) and CH_2 deformation	[36–42]
10	1313	Purine (DNA) ring vibration, $CH/CH_2/CH_3$ deformation, CH_2 wagging and twisting (lipids), minor amide III (C–N/N–H stretch)	[36, 37, 39, 41, 42]
11	1345	Purine (DNA) ring vibration, CH_2 and CH_3 deformation of collagen/proteins	[36–39, 42]
12	1405	Symmetric deformation of CH_3, ν_s(COO^-) (amino acids)	[36, 40]
13	1464	CH_2 scissoring, CH deformation (lipids), CH_2/CH_3 deformation (proteins)	[37, 38, 42, 45]
14	1512	Purine ring vibration, carotenoid ν_1 C=C stretching	[37, 42, 43]

23669608, 2026, 19, Downloaded from https://onlinelibrary.wiley.com/doi/10.1002/smtd.70972 by Hanyang University Library, Wiley Online Library on [27/10/2026]. See the Terms and Conditions (https://onlinelibrary.wiley.com/terms-and-conditions) on Wiley Online Library for rules of use; OA articles are governed by the applicable Creative Commons License

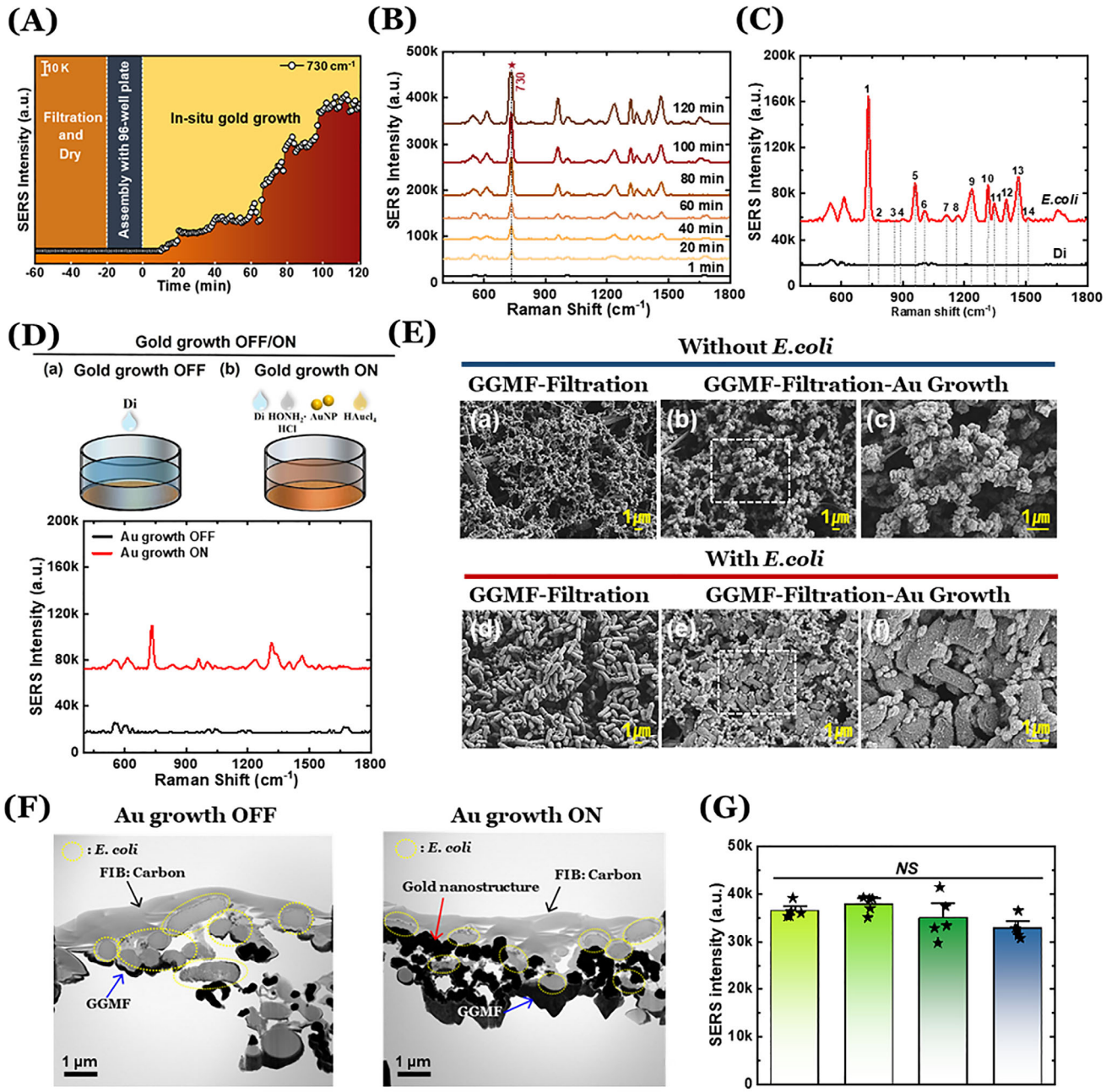

FIGURE 2 | Filtration-assisted capture of E. coli on a SERS filter membrane and subsequent in situ gold growth in the surrounding microenvironment. (A) Real-time Raman intensity at 730 cm^{-1} during in situ gold growth on the GGMF after filtration of *E. coli*. (B) Raman spectra collected at selected time points during in situ gold growth, corresponding to the real-time monitoring shown in (A). (C) Comparison of Raman spectra obtained from E. coli-filtered and DI water-filtered membranes after gold growth, highlighting distinct bacterial signatures over background. (D) Comparison of Raman spectra of E. coli-captured membranes with and without in situ gold growth (ON/OFF), confirming the essential role of gold growth for signal enhancement. (E) SEM images showing morphological evolution of GGMF membranes. (a) DI water-filtered GGMF without gold growth. (b–c) DI water-filtered GGMF after gold growth. (d) E. coli-filtered GGMF without gold growth. (e–f) E. coli-filtered GGMF after gold growth, revealing nanostructure formation in the bacterial microenvironment. (F) Cross-sectional TEM images after filtration of *E. coli* with and without subsequent in situ gold growth. (G) Averaged SERS intensity at 730 cm^{-1} for each GGMF-filtration-Au growth (mean of five spots per group). *NS* indicates no significant difference among the groups (One-way ANOVA, $p > 0.05$).

the necessity of the post-filtration growth process, comparative experiments were conducted with and without gold growth. While negligible SERS signals were observed in the absence of growth (OFF), even at a high bacterial concentration, distinct Raman peaks were clearly detected after in situ growth (ON) under otherwise identical conditions (Figure 2D). These results demonstrate that bacterial capture alone is insufficient for signal generation, and that in situ gold growth is essential for effective SERS signal amplification.

Structural evolution during the growth process was examined by SEM analysis. Minimal structural changes were observed in DI

23669608, 2026, 19, Downloaded from https://onlinelibrary.wiley.com/doi/10.1002/smtd.70972 by Hanyang University Library, Wiley Online Library on [27/10/2026]. See the Terms and Conditions (https://onlinelibrary.wiley.com/terms-and-conditions) on Wiley Online Library for rules of use; OA articles are governed by the applicable Creative Commons License

water-filtered membranes, whereas post-growth samples exhibited the formation of larger secondary nanostructures through the coalescence of pre-existing nanostructures (Figure 2E(a–c)). In the case of bacteria-captured membranes, bacteria were stably immobilized on the substrate, and additional nanostructures were observed not only on the substrate but also in the surrounding microenvironment of the bacteria after growth (Figure 2E(d–f)). To further examine the morphological features of individual bacterial cells, high-resolution SEM images were additionally analyzed (Figure S5). The magnified SEM images revealed distinct morphological differences in the bacterial surface before and after in situ Au growth. In the control group without Au growth, the bacterial surface appeared smooth, whereas after in situ Au growth, the bacterial surface became densely decorated with Au nanostructures, resulting in a markedly roughened surface morphology. The inset images further show that Au nanoparticles were uniformly distributed over the entire bacterial surface, suggesting that in situ Au growth occurred not only within the bacterial microenvironment but also directly on the bacterial cell surface. To directly verify these structural features, cross-sectional transmission electron microscopy (TEM) analysis was performed using a focused ion beam (FIB) technique (Figure 2F). In the absence of gold growth, *E. coli* cells were observed to reside relatively independently on the GGMF surface, exhibiting only simple physical contact with the substrate. In contrast, following in situ gold growth, dense gold nanostructures were formed at the bacteria–substrate interface, resulting in an interconnected hybrid architecture comprising bacteria, substrate, and gold nanostructures. Notably, gold nanostructures were preferentially concentrated at the bacterial surface and its immediate vicinity, providing direct evidence that gold growth is locally induced within the microenvironment surrounding the bacteria. These findings demonstrate that localized gold growth occurs preferentially around immobilized bacteria following filtration, enabling the formation of bacteria-centered plasmonic hotspots rather than relying solely on substrate-based hotspot generation. Consequently, this strategy effectively overcomes the hotspot–bacteria mismatch issue and enables efficient SERS signal enhancement through localized amplification within the bacterial microenvironment.

Finally, the uniformity within a single filter was validated by spot-to-spot analysis. SERS spectra collected from 30 different locations on a single filter after E. coli filtration and subsequent in situ gold growth exhibited highly consistent spectral features, with a low relative standard deviation (RSD) of 6.5%, confirming excellent within-substrate reproducibility (Figure S6). Furthermore, the overall reproducibility of the platform was evaluated across independently prepared filters and multiple measurement locations under identical conditions. Furthermore, the overall reproducibility of the platform was evaluated across independently prepared filters and multiple measurement locations under identical conditions. One-way ANOVA of the averaged SERS intensities at 730 cm^{-1} across four independent batches showed no statistically significant differences among the groups ($p = 0.06$), and the overall signal variation remained low with an RSD of 8.81%, indicating good batch-to-batch reproducibility (Figures 2G and S7). To further assess the spatial uniformity of the fabricated substrates, Raman mapping analysis was performed using five independently prepared filters. All substrates exhibited homogeneous signal distributions, with RSD values of 9.2%, 8.1%, 8.8%, 7.6%, and 6.6%, respectively, all below 10% (Figure S8). These results demonstrate that the proposed platform provides uniform SERS responses over the entire substrate surface with good batch-to-batch reproducibility.

3.3 | Selective Detection in Complex Matrices

A commonly used sample preparation method in SERS analysis involves drop-casting an analyte onto a SERS substrate followed by solvent evaporation. However, this approach has inherent limitations, including restricted sample volume due to substrate surface properties and the requirement for a drying process to remove the solvent [27]. In contrast, the GGMF-based filtration method proposed in this study enables the processing of large sample volumes and allows direct analysis without any drying step. To evaluate not only these procedural advantages but also the analytical performance, we compared the *E. coli* detection capability of the proposed method with that of the conventional drop-casting approach.

Three experimental groups were established for this comparison. The first group (a) involved drop-casting only, where TSB medium and DI water spiked with *E. coli* (1×10^7 CFU/mL) were directly deposited (20 µL) onto a SERS substrate and dried (Figure 3A). The second group (b) followed the same procedure as (a), with an additional in situ Au growth step (Figure 3B). The third group (c), representing the proposed method, involved filtration of 5 mL of the sample through the GGMF, followed by two consecutive filtration washing steps using an equal volume (5 mL) of DI water, and subsequent in situ Au growth (Figure 3C).

In the drop-casting-only condition (a), no significant Raman signal was observed from any sample, even at a high bacterial concentration (1×10^7 CFU/mL), and all spectra remained at baseline levels. This result can be attributed to the inherent dependence of SERS on localized plasmonic hotspots, where efficient signal generation requires spatial overlap between the analyte and the hotspots [b]. In this case, the limited sample volume and non-uniform distribution of bacteria on the substrate likely resulted in a low probability of hotspot–bacteria interaction, leading to a hotspot–target mismatch. In the drop-casting with Au growth condition (b), some Raman signals were observed, and *E. coli*-derived signals were distinguishable in the DI water condition. However, when *E. coli* was spiked into TSB medium, the resulting spectra exhibited significant overlap with background signals originating from the medium, making it difficult to clearly distinguish the characteristic Raman features of *E. coli*. This indicates that non-specific signals remain dominant in complex matrices, and that Au growth alone is insufficient to achieve selective detection. In contrast, the filtration-based method with Au growth (c) produced a distinct SERS spectrum characteristic of *E. coli*, including the adenine peak at 730 cm^{-1}, while effectively suppressing background signals from the medium. This trend was consistently confirmed in the quantitative analysis shown in Figure 3D, demonstrating that the filtration-based approach provides enhanced selectivity and signal resolution even in complex matrix environments.

To further evaluate this limitation in a more complex biological environment, additional control experiments were performed

23669608, 2026, 19, Downloaded from https://onlinelibrary.wiley.com/doi/10.1002/smtd.70972 by Hanyang University Library, Wiley Online Library on [27/10/2026]. See the Terms and Conditions (https://onlinelibrary.wiley.com/terms-and-conditions) on Wiley Online Library for rules of use; OA articles are governed by the applicable Creative Commons License

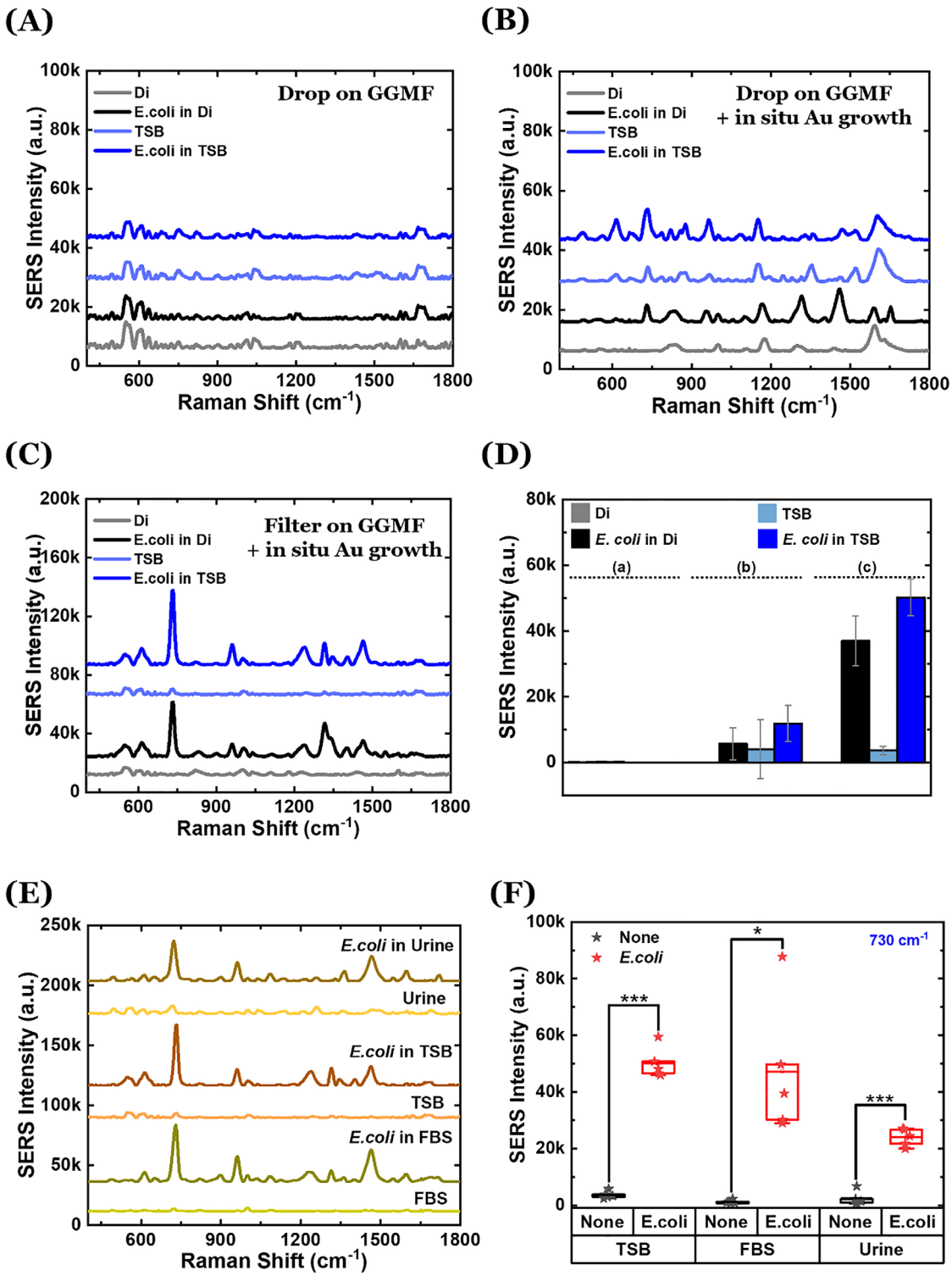

FIGURE 3 | Comparison of sample preparation methods and detection of E. coli (1×10^7 CFU/mL) using the GGMF platform in complex matrices. (A) Drop-casting only (20 μL) on a SERS substrate. (B) Drop-casting with in situ Au growth. (C) Filtration (5 mL) using GGMF, followed by two DI water filtration washing steps and in situ Au growth. (D) Raman intensity at 730 cm^{-1} (mean of five spots). (E) SERS spectra of *E. coli* (1×10^7 CFU/mL) in urine, TSB, and FBS with and without bacterial spiking using the GGMF-based method. (F) Raman intensity at 730 cm^{-1} across different matrices (mean of five spots). *$p < 0.05$ and ***$p < 0.001$ indicate statistically significant differences compared to the respective control groups (Student's *t*-test).

23669608, 2026, 19, Downloaded from https://onlinelibrary.wiley.com/doi/10.1002/smtd.70972 by Hanyang University Library, Wiley Online Library on [27/10/2026]. See the Terms and Conditions (https://onlinelibrary.wiley.com/terms-and-conditions) on Wiley Online Library for rules of use; OA articles are governed by the applicable Creative Commons License

using *E. coli* spiked into FBS, a highly complex protein-rich matrix (Figure S9). Consistent with the results obtained in the TSB matrix, the conventional drop-casting method alone failed to detect the characteristic signals of the target bacteria. Furthermore, even when in situ Au growth was applied after drop-casting, the resulting Raman signals were severely masked by strong matrix interference originating from the FBS, making accurate identification of *E. coli* impossible. These findings support that the integration of filtration-based bacterial enrichment and signal amplification within the bacterial microenvironment is essential for the accurate identification of pathogens in complex biological matrices.

The improved performance can be attributed to the combined effects of size-exclusion-based filtration and repeated DI water washing. The GGMF selectively captures bacterial cells while allowing smaller interfering molecules, such as proteins and metabolites, to pass through. In particular, the two consecutive filtration washing steps using 5 mL of DI water further remove residual non-specifically adsorbed species from the filter surface and pores, thereby minimizing background signals. Subsequent in situ Au growth occurs locally around the captured bacteria, leading to selective signal amplification.

To further evaluate selectivity under various complex biological conditions, additional experiments were conducted using TSB, FBS, and urine (Figure 3E,F). In all matrix samples without *E. coli*, no noticeable Raman signals were observed, and the spectra remained at baseline levels across the entire spectral range. In contrast, when *E. coli* was present, characteristic Raman peaks, including the adenine peak at 730 cm^{-1}, were consistently observed under all matrix conditions. These results demonstrate that the proposed platform maintains high selectivity even in complex biological environments. Notably, the Raman signal intensity varied depending on the matrix type, with the intensity at 730 cm^{-1} gradually decreasing in the order of TSB, FBS, and urine (Figure 3F). This variation is likely attributed to differences in matrix composition, which affect the level of non-specific interference and the efficiency of hotspot–bacteria interactions.

Overall, the GGMF-based filtration method, combined with in situ Au growth, not only simplifies the sample preparation process but also enables direct analysis without a drying step, while effectively suppressing background interference in complex matrices. These findings highlight the potential of the proposed platform as a reliable and selective analytical tool for rapid bacterial detection in clinically relevant samples.

3.4 | Bacterial Species Differentiation

To evaluate the species-level discrimination capability of the proposed sensor, *E. coli*, *Klebsiella* and *S. aureus* at a concentration of 1×10^7 CFU/mL were individually filtered through the GGMF, followed by in situ Au growth and SERS analysis. Distinct SERS spectra were successfully obtained from all three bacterial species. However, direct species discrimination based solely on the spectra remained challenging because the major Raman peaks overlapped owing to the structural similarity of biomolecules on the bacterial cell surfaces. To overcome this limitation, the acquired SERS spectra were normalized by scaling the maximum peak intensity to one (Max = 1), followed by PCA. After normalization, subtle differences in the Raman fingerprints among the three bacterial species became more apparent (Figure S10). The PCA score plot showed that the three bacterial species formed well-separated and distinct clusters. In addition, 95% confidence ellipses exhibited minimal overlap among the clusters, indicating good reproducibility and clear separation of the spectral data. These results demonstrate that the proposed platform can effectively discriminate bacterial species based on their characteristic Raman fingerprints.

3.5 | Overcoming Sampling Limitations for SERS Detection at Low Bacterial Concentrations

At low bacterial concentrations, the detection limit is governed not only by the intrinsic analytical sensitivity of the sensing platform, but also by the probability that bacterial cells are present within the laser interrogation area after filtration. In SERS-based measurements, signals are generated from highly localized regions on the order of several μm^2, making the spatial distribution of bacteria inherently stochastic. Under such conditions, even when bacteria are present in the bulk sample, the probability that they are located within the laser-probed area becomes increasingly limited at low concentrations, often resulting in false-negative signals. Therefore, in the low concentration regime, detection performance is dictated not only by sensitivity but also by the spatial occupancy of bacterial cells within the detection region.

To address this sampling limitation, a minimal pre-culture step was introduced prior to filtration. This strategy enables a modest increase in bacterial number, thereby enhancing surface occupancy on the filter and increasing the likelihood of bacterial presence within the laser interrogation area. In addition, the subsequent in situ gold growth process forms localized plasmonic nanostructures around bacterial surfaces, further increasing the density of electromagnetic hotspots within the bacterial microenvironment.

To optimize the minimal culture duration, *E. coli* at an initial concentration of 1×10^4 CFU/mL was cultured in TSB+FBS (1:1, total volume 5 mL) for 0–4 h, followed by filtration through GGMF, two DI washing steps, and in situ gold growth prior to SERS measurement. The doubling time of *E. coli* is known to be approximately 15–30 min, indicating that even a short 1 h culture can result in a 4–16-fold increase in bacterial population [28]. As shown in Figure 4A,B, the intensity of the 730 cm^{-1} peak increased progressively with culture time and reached a plateau at approximately 2 h. This trend is attributed to increased surface occupancy and a higher probability of hotspot–bacteria interactions resulting from bacterial proliferation. In contrast, a decrease in signal intensity was observed after 3 h of culture. This reduction is likely due to excessive bacterial accumulation leading to aggregation and overlap on the filter surface, which can hinder plasmonic hotspot accessibility and induce electromagnetic field screening effects. Furthermore, overcrowding may disrupt the uniform formation of gold nanostructures, thereby reducing the reproducibility of hotspot generation. Considering the need for rapid diagnostics, a 1 h culture duration was selected as the optimal condition, as it provides a sufficient increase in

23669608, 2026, 19, Downloaded from https://onlinelibrary.wiley.com/doi/10.1002/smtd.70972 by Hanyang University Library, Wiley Online Library on [27/10/2026]. See the Terms and Conditions (https://onlinelibrary.wiley.com/terms-and-conditions) on Wiley Online Library for rules of use; OA articles are governed by the applicable Creative Commons License

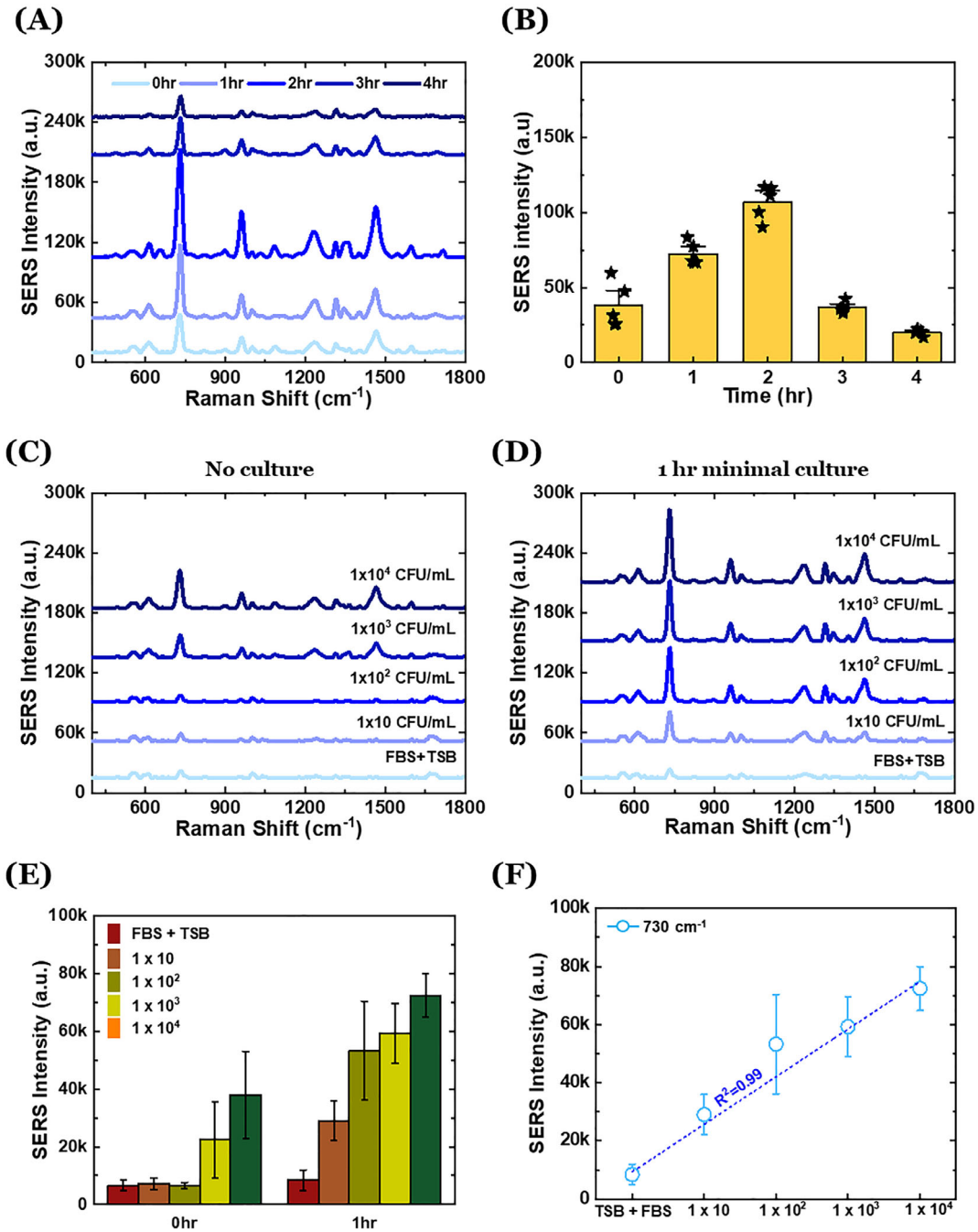

FIGURE 4 | Evaluation of culture time optimization and limit of detection (LOD) of the GGMF-based SERS platform for *E. coli*. (A, B) Raman spectra and corresponding intensity analysis at ~730 cm^{-1} obtained from E. coli at an initial concentration of 1×10^4 CFU/mL after varying culture durations (0–4 h) prior to filtration and in situ gold growth (mean of five spots). (C) Raman spectra acquired at different bacterial concentrations without pre-culture. (D) Raman spectra obtained at varying bacterial concentrations after 1 h culture. (E) Quantitative analysis of Raman intensity at ~730 cm^{-1} for both non-cultured and 1 h cultured samples (mean of five spots). (F) Linear calibration curve based on Raman intensity at ~730 cm^{-1} for the 1 h cultured samples (mean of five spots).

bacterial population while avoiding signal degradation due to overaccumulation.

Notably, in the absence of pre-culture, detection performance was evaluated over a concentration range of 1×10^1–1×10^4 CFU/mL, yielding a limit of detection (LOD) of approximately 10^3 CFU/mL (Figure 4C,E). This result demonstrates that the platform is capable of directly covering clinically relevant bacterial concentrations, particularly those associated with UTIs, without the need for additional amplification steps.

Upon applying the optimized 1 h culture condition, detection performance was re-evaluated over the same concentration range (1×10^1–1×10^4 CFU/mL). As shown in Figure 4D–F, SERS spectra (Figure 4D), peak intensity analysis (Figure 4E), and linear regression (Figure 4F) consistently exhibited a concentration-

23669608, 2026, 19, Downloaded from https://onlinelibrary.wiley.com/doi/10.1002/smtd.70972 by Hanyang University Library, Wiley Online Library on [27/10/2026]. See the Terms and Conditions (https://onlinelibrary.wiley.com/terms-and-conditions) on Wiley Online Library for rules of use; OA articles are governed by the applicable Creative Commons License

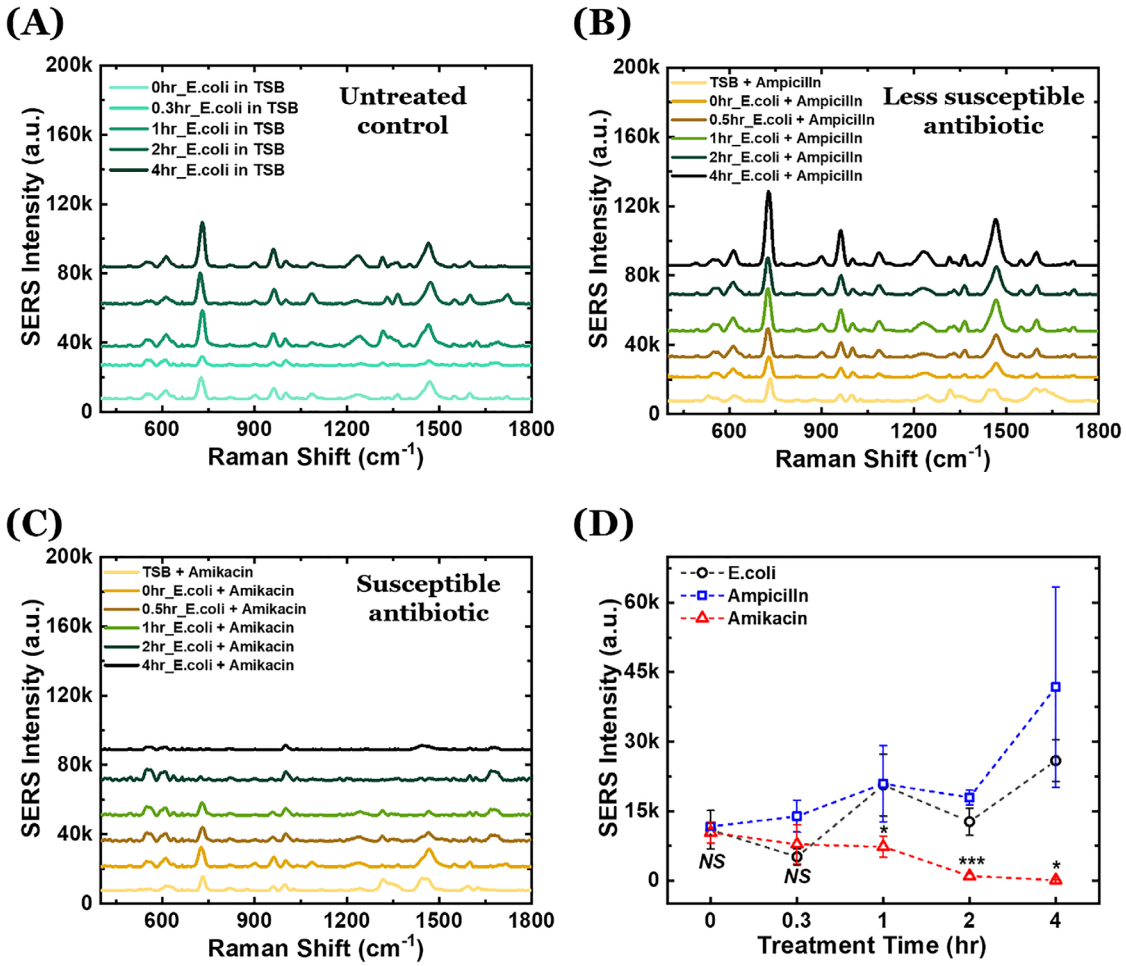

FIGURE 5 | Rapid antimicrobial susceptibility testing based on time-dependent SERS responses. Time-resolved SERS spectra of E. coli (1×10^3 CFU/mL) in TSB under different conditions: (A) untreated control, (B) ampicillin-treated (less susceptible antibiotic), and (C) amikacin-treated (susceptible antibiotic). (D) Quantitative analysis of the Raman intensity at 730 cm^{-1} from (A–C), averaged over five measurement spots. Error bars represent standard deviation ($n = 5$). ***$p < 0.001$ indicates a statistically significant difference between the amikacin-treated group and the untreated E. coli control group (One-way ANOVA with Tukey's post hoc test).

dependent increase in signal intensity. In particular, the intensity of the 730 cm^{-1} peak showed excellent linear correlation with bacterial concentration ($R^2 = 0.98$), confirming the quantitative capability of the platform.

Importantly, clear SERS signals were detectable even at an low concentration of 1×10^1 CFU/mL. This improvement arises not only from analytical sensitivity, but also from an increased probability of bacterial presence within the laser interrogation area, enabled by minimal pre-culture–induced enhancement of surface occupancy. By mitigating the inherent sampling limitation of SERS at low concentrations, this approach substantially improves practical detectability. Consequently, the platform enables rapid detection across clinically relevant bacterial concentrations for UTI (10^2–10^3 CFU/mL), while extending detection capability down to 10^1 CFU/mL [29]. This performance highlights its potential for both routine infection diagnostics and early-stage detection scenarios, such as sepsis, where bacterial loads are extremely low [30].

3.6 | Rapid AST via SERS-Based Viability Assessment

Accurate assessment of antimicrobial susceptibility is essential for guiding patient-specific antibiotic therapy. However, conventional AST relies on bacterial culture, requiring several days to obtain results and often involving bulky laboratory equipment, thereby limiting its applicability in point-of-care testing (POCT) settings [31, 32]. In this study, we extended the previously optimized minimal culture–based detection strategy to an antibiotic response system, enabling rapid AST through SERS-based viability assessment using the GGMF platform (Figure 5).

To simulate clinically relevant conditions, *E. coli* at a low initial concentration (1×10^3 CFU/mL) was suspended in TSB medium and treated with two representative antibiotics: amikacin, to which *E. coli* is highly susceptible, and ampicillin, for which *E. coli* typically exhibits reduced susceptibility or resistance [33, 34]. The mixtures were incubated at 37°C for 0, 0.5, 1, 2, and 4 h,

23669608, 2026, 19, Downloaded from https://onlinelibrary.wiley.com/doi/10.1002/smtd.70972 by Hanyang University Library, Wiley Online Library on [27/10/2026]. See the Terms and Conditions (https://onlinelibrary.wiley.com/terms-and-conditions) on Wiley Online Library for rules of use; OA articles are governed by the applicable Creative Commons License

TABLE 2 | Comparison of representative bacterial detection methods.

Feature	Culture-based methods	PCR	MALDI-TOF MS	Conventional SERS	This work
Turnaround time	24–72 h	2–4 h	< 1 h (after culture)	30–120 min	< 30 min
Sample pretreatment	None	DNA extraction	Bacterial culture required	Centrifugation and/or purification	GGMF filtration only
Direct analysis in complex biological matrices	Limited	Limited	No	Limited	Yes
Species identification	Yes	Yes	Yes	Yes	Yes
Antimicrobial susceptibility testing (AST)	Yes	No	No	Limited	Yes
Label-free detection	Yes	No	Yes	Yes	Yes

and bacterial responses were evaluated via time-dependent SERS measurements.

As shown in Figure 5A–C, distinct temporal SERS responses were observed depending on antibiotic treatment. In the untreated control group (Figure 5A), the SERS intensity progressively increased with incubation time, reflecting bacterial proliferation. This increase is attributed to both the rise in bacterial population and the enhanced probability of hotspot–bacteria interactions due to increased surface occupancy following in situ gold growth. The Raman peak at 730 cm^{-1}, associated with adenine-related intracellular components, served as a reliable indicator of bacterial presence and metabolic activity. In the ampicillin-treated group (Figure 5B), a similar increasing trend in SERS intensity was observed, indicating that bacterial growth was not effectively inhibited. As a β-lactam antibiotic, ampicillin interferes with cell wall synthesis; however, *E. coli* often exhibits resistance through mechanisms such as β-lactamase production or modification of penicillin-binding proteins [34]. This reduced susceptibility is directly reflected in the sustained increase of SERS signals over time. In contrast, the amikacin-treated group (Figure 5C) exhibited a markedly different response. A rapid decrease in SERS intensity was observed starting at 30 min, with signals nearly disappearing after 2 h. Amikacin, an aminoglycoside antibiotic, exerts a bactericidal effect by inhibiting protein synthesis, leading to rapid cell death [35]. This results in a decrease in viable bacterial cells and a corresponding reduction in bacteria-associated plasmonic hotspot formation, ultimately leading to a pronounced loss of SERS signal. To quantitatively compare these responses, the intensity of the 730 cm^{-1} peak was plotted as a function of incubation time (Figure 5D). The divergence among the control, ampicillin-treated, and amikacin-treated groups became most pronounced at 2 h, indicating that this time point provides optimal discrimination between susceptible and resistant phenotypes. Accordingly, 2 h was selected as the optimal reaction time for rapid antimicrobial susceptibility assessment. Statistical analysis (Tukey's test) showed that the amikacin-treated group exhibited a statistically significant reduction in SERS intensity compared with the untreated control after 1 h ($p < 0.05$) and was therefore classified as susceptible. In contrast, the ampicillin-treated group exhibited a statistically significant increase in SERS intensity over time compared with the untreated control ($p < 0.05$). These results indicate that bacterial strains with different levels of antibiotic susceptibility exhibit distinct SERS responses following antibiotic treatment.

These results demonstrate that SERS signal intensity in this platform can serve as a direct indicator of bacterial viability. Unlike conventional approaches that rely on prolonged culture-based growth measurements, the proposed method enables rapid differentiation of antimicrobial responses based on short-term changes in viability. Overall, the GGMF-based platform allows reliable antimicrobial susceptibility determination within a 2 h total processing time (including reaction and culture), representing a substantial reduction in analysis time compared to conventional AST. Furthermore, given its minimal instrumentation requirements and compatibility with rapid diagnostic workflows, this approach holds strong potential for application in clinical and POCT settings.

As summarized in Table S2, the proposed GGMF-integrated in situ SERS platform compares favorably with representative state-of-the-art SERS-based bacterial detection platforms. Although filtration-, magnetic-, and aptamer-based SERS platforms have achieved high detection sensitivity, many still require additional enrichment or separation procedures and have limited applicability for the direct analysis of large-volume complex biological matrices. In contrast, the proposed platform enables direct bacterial enrichment and detection from complex biological matrices through GGMF-assisted filtration without additional sample pretreatment, while also integrating rapid bacterial detection and AST within a single platform. In addition, comparison with conventional bacterial diagnostic methods (Table 2) further highlights the practical advantages of the proposed platform. Unlike culture-based methods, PCR, and MALDI-TOF MS, which typically require prolonged culture, DNA extraction, or multiple analytical steps, the proposed

23669608, 2026, 19, Downloaded from https://onlinelibrary.wiley.com/doi/10.1002/smtd.70972 by Hanyang University Library, Wiley Online Library on [27/10/2026]. See the Terms and Conditions (https://onlinelibrary.wiley.com/terms-and-conditions) on Wiley Online Library for rules of use; OA articles are governed by the applicable Creative Commons License

platform provides a simple workflow for direct bacterial enrichment, identification, and AST, making it well suited for rapid infectious disease diagnostics and future point-of-care applications.

This study presents a proof-of-concept demonstrating the simultaneous implementation of low-level bacterial detection and rapid AST using *E. coli*, highlighting the potential of the GGMF platform as an integrated diagnostic system. Future studies are required to systematically evaluate its capture efficiency across a broader range of bacterial species, which will be essential for establishing its general applicability. In addition, with recent advances in label-free data-driven analysis and artificial intelligence (AI)-based classification techniques, distinct SERS spectral signatures are expected to enable precise discrimination among diverse pathogens [46]. Such an approach would enable the integration of multiplex pathogen detection with antimicrobial susceptibility assessment, ultimately advancing this platform toward a next-generation diagnostic system capable of supporting rapid and accurate clinical diagnosis and therapeutic decision-making.

4 | Conclusion

In this study, we developed a filtration-based SERS platform that enables efficient capture and enrichment of bacteria from large-volume samples, followed by localized plasmonic nanostructure formation within the bacterial microenvironment. By integrating physical enrichment with in situ gold growth, the proposed system establishes a bacteria-centered plasmonic architecture that effectively overcomes the spatial mismatch between nanoscale hotspots and microscale bacterial targets, enabling stable and reproducible signal generation. Importantly, this work highlights that detection performance at low concentrations is governed not only by signal amplification efficiency but also by sampling limitations associated with bacterial distribution. By introducing a minimal pre-culture step to enhance bacterial surface occupancy, these limitations were effectively addressed, allowing reliable detection under clinically relevant low-concentration conditions. Furthermore, the direct coupling between plasmonic signal generation and bacterial viability enables rapid functional assessment of antimicrobial responses, supporting susceptibility determination within a significantly reduced time frame compared to conventional culture-based methods. While this study demonstrates the technological feasibility of the proposed platform as a proof-of-concept, validation using authentic clinical specimens remains necessary to establish its clinical applicability. Future studies will focus on evaluating patient-derived samples and expanding the Raman spectral database to include a broader range of clinically relevant bacterial species, together with AI-based analytical approaches for accurate bacterial identification in complex clinical specimens. Taken together, this study demonstrates that integrating filtration-assisted enrichment with in situ Au nanostructure growth in the bacterial microenvironment provides a practical and effective strategy for sensitive and selective bacterial detection in complex biological matrices. This approach offers a promising foundation for the development of next-generation diagnostic platforms that combine low-level detection with rapid functional analysis for clinical applications.

Author Contributions

Eun-Bi Jang: investigation, data curation, methodology, conceptualization, Writing – original draft. **Ji Young Lee**: *E. coli* sampling and SEM measurement. **Hoeil Chung**: supervision, **Min-Young Lee**: investigation, conceptualization, writing – review & editing, supervision, project administration.

Acknowledgements

This study was supported by the Technology Innovation Program (RS-2024-00432381) funded by the Ministry of Trade, Industry & Energy (MOTIE, Korea), and the Fundamental Research Program (PNKB010) of the Korea Institute of Materials Science (KIMS). This research was supported by the National Research Council of Science & Technology (NST) grant by the Korea government (MSIT) (No. GTL25061-000).

Conflicts of Interest

The authors declare that they have no known competing financial interests or personal relationships that could have appeared to influence the work reported in this paper.

Data Availability Statement

The data that support the findings of this study are available from the corresponding author upon reasonable request.

References

1. C. Tian, L. Zhao, G. Qi, and S. Zhang, "Trace Detection of E. coli O157:H7 Cells by an Au Nanoparticle-Based SERS Aptasensor," *ACS Applied Nano Materials* 6 (2023): 1386–1394, https://doi.org/10.1021/acsanm.2c05031.

2. S. Park, K. Kim, A. Go, M.-H. Lee, L. Chen, and J. Choo, "Rapid and Sensitive *Escherichia coli* Detection: Integration of SERS and Acoustofluidics in a Lysis-Free Microfluidic Platform," *ACS Sensors* 10 (2025): 1217–1227, https://doi.org/10.1021/acssensors.4c03118.

3. W. R. Premasiri, Y. Chen, P. M. Williamson, D. C. Bandarage, C. Pyles, and L. D. Ziegler, "Rapid Urinary Tract Infection Diagnostics by Surface-Enhanced Raman Spectroscopy (SERS): Identification and Antibiotic Susceptibilities," *Analytical and Bioanalytical Chemistry* 409 (2017): 3043–3054, https://doi.org/10.1007/s00216-017-0244-7.

4. L. Samuel, "Direct-From-Blood Detection of Pathogens: A Review of Technology and Challenges," *Journal of Clinical Microbiology* 61 (2023): e00231, https://doi.org/10.1128/jcm.00231-21.

5. B. Sequeira-Antunes and H. A. Ferreira, "Urinary Biomarkers and Point-of-Care Urinalysis Devices for Early Diagnosis and Management of Disease: A Review," *Biomedicines* 11 (2023): 1051, https://doi.org/10.3390/biomedicines11041051.

6. A. Afshari, J. Schrenzel, M. Ieven, and S. Harbarth, "Bench-to-Bedside Review: Rapid Molecular Diagnostics for Bloodstream Infection—A New Frontier?," *Critical Care* 16 (2012): 222, https://doi.org/10.1186/cc11202.

7. A. Ahmed, J. V. Rushworth, N. A. Hirst, and P. A. Millner, "Biosensors for Whole-Cell Bacterial Detection," *Clinical Microbiology Reviews* 27 (2014): 631–646, https://doi.org/10.1128/cmr.00120-13.

8. E. Avershina, A. Khezri, and R. Ahmad, "Clinical Diagnostics of Bacterial Infections and Their Resistance to Antibiotics—Current State and Whole Genome Sequencing Implementation Perspectives," *Antibiotics* 12 (2023): 781, https://doi.org/10.3390/antibiotics12040781.

9. R. P. Bhattacharyya, N. Bandyopadhyay, P. Ma, et al., "Simultaneous Detection of Genotype and Phenotype Enables Rapid and Accurate Antibiotic Susceptibility Determination," *Nature Medicine* 25 (2019): 1858–1864, https://doi.org/10.1038/s41591-019-0650-9.

23659608, 2026, 19, Downloaded from https://onlinelibrary.wiley.com/doi/10.1002/smtd.70972 by Hanyang University Library, Wiley Online Library on [27/10/2026]. See the Terms and Conditions (https://onlinelibrary.wiley.com/terms-and-conditions) on Wiley Online Library for rules of use; OA articles are governed by the applicable Creative Commons License

10. R. Banerjee and R. Patel, "Molecular Diagnostics for Genotypic Detection of Antibiotic Resistance: Current Landscape and Future Directions," *JAC-Antimicrobial Resist* 5 (2023): dlad018, https://doi.org/10.1093/jacamr/dlad018.

11. Y. Liu, H. Zhou, Z. Hu, G. Yu, D. Yang, and J. Zhao, "Label and Label-Free Based Surface-Enhanced Raman Scattering for Pathogen Bacteria Detection: A Review," *Biosensors & Bioelectronics* 94 (2017): 131–140, https://doi.org/10.1016/j.bios.2017.02.032.

12. M. Usman, J.-W. Tang, F. Li, et al., "Recent Advances in Surface Enhanced Raman Spectroscopy for Bacterial Pathogen Identifications," *Journal of Advanced Research* 51 (2023): 91–107, https://doi.org/10.1016/j.jare.2022.11.010.

13. X. Zhou, Z. Hu, D. Yang, et al., "Bacteria Detection: From Powerful SERS to Its Advanced Compatible Techniques," *Advanced Science* 7 (2020): 2001739, https://doi.org/10.1002/advs.202001739.

14. S. D. Dryden, S. Anastasova, G. Satta, A. J. Thompson, D. R. Leff, and A. Darzi, "Rapid Uropathogen Identification Using Surface Enhanced Raman Spectroscopy Active Filters," *Scientific Reports* 11 (2021): 8802, https://doi.org/10.1038/s41598-021-88026-9.

15. Y. Yang, X. Chen, B. Ai, and Y. Zhao, "The Impact of Analyte Size on SERS Enhancement Location, Enhancement Factor, Excitation Wavelength, and Spectrum," *Sensors and Diagnostics* 3 (2024): 668–676, https://doi.org/10.1039/d4sd00014e.

16. N. G. Bastús, J. Comenge, and V. Puntes, "Kinetically Controlled Seeded Growth Synthesis of Citrate-Stabilized Gold Nanoparticles of up to 200 Nm: Size Focusing Versus Ostwald Ripening," *Langmuir* 27 (2011): 11098–11105, https://doi.org/10.1021/la201938u.

17. J. Y. Kim, E. H. Koh, J. Yang, et al., "3D Plasmonic Gold Nanopocket Structure for SERS Machine Learning-Based Microplastic Detection," *Advanced Functional Materials* 34 (2024): 2307584, https://doi.org/10.1002/adfm.202307584.

18. S. P. Asrafali, T. Periyasamy, S.-C. Kim, and J.-W. Lee, "Enhanced Wettability and Adhesive Property of PTFE Through Surface Modification With Fluorinated Compounds," *Materials* 17 (2024): 3051, https://doi.org/10.3390/ma17133051.

19. Q. Han and Y. Kang, "Separation of Water-In-Oil Emulsion With Microfiber Glass Coalescing Bed," *Journal of Dispersion Science and Technology* 38 (2017): 1523–1529, https://doi.org/10.1080/01932691.2016.1259073.

20. Z. A. Ansari, F. Arshad, L. D. Nghiem, and L. Zou, "Amphiphilic Cellulose Acetate Membrane Incorporated With MoS_2 Nanospheres for Oil in Water Separation," *Environmental Science: Water Research & Technology* 8 (2022): 2694–2704, https://doi.org/10.1039/d2ew00385f.

21. L.-Y. Wang, Y.-H. Zhang, and L.-J. Zhao, "Raman Spectroscopic Studies on Single Supersaturated Droplets of Sodium and Magnesium Acetate," *Journal of Physical Chemistry A* 109 (2005): 609–614, https://doi.org/10.1021/jp0458811.

22. M.-J. Kim, K. Yang, H.-J. Kang, et al., "Polyimide-Coated Glass Microfiber as Polysulfide Perm-Selective Separator for High-Performance Lithium-Sulphur Batteries," *Nanomaterials* 9 (2019): 1612, https://doi.org/10.3390/nano9111612.

23. L. O. Migliarini, S. M. Landro, F. Martinez-Espinoza, D. H. Murgida, and F. Arrighetti, "Profiling Microplastic Fibers in the Intertidal Sentinel Mussel *Brachidontes rodriguezii* From the Coast of Buenos Aires, Argentina," *PeerJ* 13 (2025): 19518, https://doi.org/10.7717/peerj.19518.

24. F. Huo and Y. Lu, "Homogeneous Synthesis of Hydroxylamine Hydrochloride via Acid-Catalyzed Hydrolysis of Nitromethane," *Reaction Chemistry & Engineering* 5 (2019): 387–394, https://doi.org/10.1039/c9re00468h.

25. İ. Gözeten and K. Karakaş, "Copper Nanoparticles Impregnated on Halloysite Support: A Highly Active, Flexible and Reusable Heterogeneous Nanocatalyst in the Reduction of 4-Nitrophenol Under Mild Conditions," *Journal of Water Process Engineering* 80 (2025): 109138, https://doi.org/10.1016/j.jwpe.2025.109138.

26. P. Kubryk, R. Niessner, and N. P. Ivleva, "The Origin of the Band at Around 730 cm^{-1} in the SERS Spectra of Bacteria: A Stable Isotope Approach," *Analyst* 141 (2016): 2874–2878, https://doi.org/10.1039/c6an00306k.

27. R. K. Sinha, "A Highly Sensitive Surface-Enhanced Raman Scattering Substrate Prepared on a Hydrophobic Surface Using Controlled Evaporation," *RSC Advances* 12 (2021): 331–337, https://doi.org/10.1039/d1ra07871b.

28. B. Gibson, D. J. Wilson, E. Feil, and A. Eyre-Walker, "The Distribution of Bacterial Doubling Times in the Wild," *Proceedings of the Royal Society* 285 (2018): 20180789, https://doi.org/10.1098/rspb.2018.0789.

29. A. A. van Driel, D. W. Notermans, A. Meima, et al., "Antibiotic Resistance of *Escherichia coli* Isolated From Uncomplicated UTI in General Practice Patients Over a 10-Year Period," *European Journal of Clinical Microbiology & Infectious Diseases* 38 (2019): 2151–2158, https://doi.org/10.1007/s10096-019-03655-3.

30. J. Shin, G. S. Kim, S. Ha, et al., "Artificially Intelligent Nasal Perception for Rapid Sepsis Diagnostics," *NPJ Digital Medicine* 8 (2025): 476, https://doi.org/10.1038/s41746-025-01851-4.

31. I. Gajic, J. Kabic, D. Kekic, et al., "Antimicrobial Susceptibility Testing: A Comprehensive Review of Currently Used Methods," *Antibiotics* 11 (2022): 427, https://doi.org/10.3390/antibiotics11040427.

32. N. E. Dina, M. A. Tahir, S. Z. Bajwa, I. Amin, V. K. Valev, and L. Zhang, "SERS-Based Antibiotic Susceptibility Testing: Towards Point-of-Care Clinical Diagnosis," *Biosensors & Bioelectronics* 219 (2023): 114843, https://doi.org/10.1016/j.bios.2022.114843.

33. J. L. Kuti, Q. Wang, H. Chen, H. Li, H. Wang, and D. P. Nicolau, "Defining the Potency of Amikacin Against *Escherichia coli*, *Klebsiella pneumoniae*, *Pseudomonas aeruginosa*, and *Acinetobacter baumannii* Derived From Chinese Hospitals Using CLSI and Inhalation-based Breakpoints," *Infection and Drug Resistance* 11 (2018): 783–790, https://doi.org/10.2147/idr.s161636.

34. M. Li, Q. Liu, Y. Teng, et al., "The Resistance Mechanism of Escherichia Coli Induced by Ampicillin in Laboratory," *Infection and Drug Resistance* 12 (2019): 2853–2863, https://doi.org/10.2147/idr.s221212.

35. A. Raut, D. Sharma, and V. Suvarna, "A Status Update on Pharmaceutical Analytical Methods of Aminoglycoside Antibiotic: Amikacin," *Critical Reviews in Analytical Chemistry* 52 (2022): 375–391, https://doi.org/10.1080/10408347.2020.1803042.

36. N. Paccotti, F. Boschetto, S. Horiguchi, et al., "Label-Free SERS Discrimination and in Situ Analysis of Life Cycle in *Escherichia coli* and *Staphylococcus epidermidis*," *Biosensors* 8 (2018): 131, https://doi.org/10.3390/bios8040131.

37. W. E. Huang, M. Li, R. M. Jarvis, R. Goodacre, and S. A. Banwart, "Chapter 5 Shining Light on the Microbial World the Application of Raman Microspectroscopy," *Advances in Applied Microbiology* 70 (2010): 153–186, https://doi.org/10.1016/s0065-2164(10)70005-8.

38. M. Kashif, M. I. Majeed, H. Nawaz, et al., "Surface-enhanced Raman Spectroscopy for Identification of Food Processing Bacteria," *Spectrochimica Acta Part A: Molecular and Biomolecular Spectroscopy* 261 (2021): 119989, https://doi.org/10.1016/j.saa.2021.119989.

39. H. Hu, J. Wang, X. Yi, et al., "Stain-Free Gram Staining Classification of Pathogens via Single-Cell Raman Spectroscopy Combined With Machine Learning," *Analytical Methods* 14 (2022): 4014–4020, https://doi.org/10.1039/d2ay01056a.

40. S. Uusitalo, M. Kögler, A.-L. Välimaa, et al., "Detection of *Listeria Innocua* on Roll-to-Roll Produced SERS Substrates With Gold Nanoparticles," *RSC Advances* 6 (2016): 62981–62989, https://doi.org/10.1039/c6ra08313g.

41. C. Fan, Z. Hu, A. Mustapha, and M. Lin, "Rapid Detection of Food- and Waterborne Bacteria Using Surface-Enhanced Raman Spectroscopy Coupled With Silver Nanosubstrates," *Applied Microbiology and Biotechnology* 92 (2011): 1053–1061, https://doi.org/10.1007/s00253-011-3634-3.

23669608, 2026, 19, Downloaded from https://onlinelibrary.wiley.com/doi/10.1002/smtd.70972 by Hanyang University Library, Wiley Online Library on [27/10/2026]. See the Terms and Conditions (https://onlinelibrary.wiley.com/terms-and-conditions) on Wiley Online Library for rules of use; OA articles are governed by the applicable Creative Commons License

42. F. S. de S Oliveira, A. M. da Silva, M. T. T. Pacheco, H. E. Giana, and L. Silveira, "Biochemical Characterization of Pathogenic Bacterial Species Using Raman Spectroscopy and Discrimination Model Based on Selected Spectral Features," *Lasers in Médical Science* 36 (2021): 289–302, https://doi.org/10.1007/s10103-020-03028-9.

43. J. Udensi, J. Loughman, E. Loskutova, and H. J. Byrne, "Raman Spectroscopy of Carotenoid Compounds for Clinical Applications—A Review," *Molecules* 27 (2022): 9017, https://doi.org/10.3390/molecules27249017.

44. L. Zeiri, B. V. Bronk, Y. Shabtai, J. Eichler, and S. Efrima, "Surface-Enhanced Raman Spectroscopy as a Tool for Probing Specific Biochemical Components in Bacteria," *Applied Spectroscopy* 58 (2003): 33–40, https://doi.org/10.1366/000370204322729441.

45. D. Lin-Vien, N. B. Colthup, W. G. Fateley, and J. G. Grasselli, *The Handbook of Infrared and Raman Characteristic Frequencies of Organic Molecules* (Academic Press, 1991), 9–28, https://doi.org/10.1016/b978-0-08-057116-4.50008-0.

46. J. W. Tang, Q. Yuan, X. R. Wen, M. Usman, A. C. Y. Tay, and L. Wang, "Label-Free Surface-Enhanced Raman Spectroscopy Coupled With Machine Learning Algorithms in Pathogenic Microbial Identification: Current Trends, Challenges, and Perspectives," *Interdisciplinary Medicine* 2 (2024): 20230060, https://doi.org/10.1002/INMD.20230060.

Supporting Information

Additional supporting information can be found online in the Supporting Information section.

Supporting File: smtd70972-sup-0001-SuppMat.docx.

23669608, 2026, 19, Downloaded from https://onlinelibrary.wiley.com/doi/10.1002/smtd.70972 by Hanyang University Library, Wiley Online Library on [27/10/2026]. See the Terms and Conditions (https://onlinelibrary.wiley.com/terms-and-conditions) on Wiley Online Library for rules of use; OA articles are governed by the applicable Creative Commons License